JBC RESEARCH ARTICLE

Hydrophobicity-tuned anion responsiveness underlies endosomolytic cargo delivery mediated by amphipathic vehicle peptides

Received for publication, August 13, 2021, and in revised form, October 26, 2021 Published, Papers in Press, November 2, 2021,
https://doi.org/10.1016/j.jbc.2021.101364

Xiaolong Chen[1,2], **Hanjie Liu**[1,2], **Ang Li**[1,2], **Shuangshuang Ji**[1,2], **and Hao Fei**[1,2,*]

From the [1]*CAS Key Laboratory of Nano-Bio Interface, Division of Nanobiomedicine, Suzhou Institute of Nano-Tech and Nano-Bionics, Chinese Academy of Sciences, Suzhou, China;* [2]*School of Nano-Tech and Nano-Bionics, University of Science and Technology of China, Hefei, China*

Edited by Phyllis Hanson

Peptide conformation can change subject to environment cues. This concept also applies to many cationic amphipathic peptides (CAPs) known to have cell membrane lytic or penetrative activities. Well-conditioned CAPs can match the properties of the target membrane to support their intended biological functions, *e.g.*, intracellular cargo delivery; however, the intricacy in such conditioning surpasses our current understanding. Here we focused on hydrophobicity, a key biophysical property that dictates the membrane activity of CAPs, and applied a structure–function strategy to evolve a template peptide for endosomolytic cargo delivery. The template was subjected to iterative adjustment to balance hydrophobicity between its N-terminal linear and C-terminal helical domains. We demonstrate that the obtained peptide, LP6, could dramatically promote cargo cell entry and facilitate cytosolic delivery of biomacromolecules such as FITC-dextran, saporin, and human IgG. Among the evolved peptide series, LP6 has low cytotoxicity and moderate hydrophobicity, exhibits maximum change in helical conformation in response to negatively charged phospholipids, and also shows an apparent aggregational behavior in response to sialic acid enrichment. These attributes of LP6 collectively indicate that its anion-responsive conformational change is a critical underlining of its endosomolytic cargo delivery capability. Our results also suggest that modulation of hydrophobicity serves as a key to the precise tuning of CAP's membrane activity for future biomedical applications.

Cationic peptides as one of the most well-studied classes of membrane-active peptides may serve as promising "vehicles" for intracellular delivery of biomacromolecules (1–3). Traditionally, cationic membrane active peptides are classified as "penetrative" or "lytic" based on their mechanisms of actions (4–6). For example, a class of cell-penetrating peptides (CPP) represented by TAT or oligoarginines can mediate cell entry of biomacromolecules in a penetrative manner *via* energy-independent direct translocation or energy-dependent endocytosis (7–9). This delivery modality however requires covalent conjugation of CPP to the cargo and often faces challenge of low endosomal escape efficiency (10, 11), both of which hinder its wide application. Another major class of cationic peptides are characterized by their amphipathic structures and ability to lyse the lipid bilayer of plasma or organelle membranes, as represented by numerous host defense peptides (12–16). Generally, when the applied concentrations exceed certain thresholds, these peptides would undergo self-aggregation and cause membrane rupture and cell death (17–19). Some of the peptides have therefore been explored as candidates of anticancer agents (20, 21). However, the cell death caused by such excessive membrane activity is undesirable for intracellular delivery purposes.

In an ideal scenario, the delivery process should firstly be initiated by vehicle peptide escorting the cargos into cells without causing direct damage to the cell membrane and then be followed by endosomal membrane lysis for cargo release into the cytosol (22–24). Yet, it remains a challenge to devise peptides with well-controlled membrane activities to achieve such selective membrane actions. Recently, studies have uncovered a more subtle boundary between "penetrative" and "lytic" modes of membrane action of cationic peptides for entering cells (25). Delicate control of hydrophobicity appeared critical for an environment-sensitive switch between the two modes of action by these peptides (26, 27). The hydrophobic domain can manifest in two structural forms, one as a string of continuous hydrophobic residues in a linear structure (28, 29), or two as intermittently distributed hydrophobic residues forming continuous surface in an amphipathic secondary structure (30–32). Interestingly, many naturally occurring amphipathic antimicrobial peptides adopt both forms of these structures, usually in a scheme of N-terminal hydrophobic domain followed by a C-terminal helical amphipathic domain (33–35). We speculate that in these peptides, the N-term hydrophobic segments prime their membrane association and the C-term helical regions further assemble to cause membrane lysis.

In a previous effort to explore how the balance of hydrophobicity affects cationic amphipathic peptides' cytotoxicity, a series of single-site mutants based on model template KL1 (KLLKLLKKLLKLLK-amide) were designed (27). These

* For correspondence: Hao Fei, hfei2008@sinano.ac.cn.

peptides exhibit nonlytic mode of membrane action. Among them, L9E (KLLKLLKKELKLLK-amide) showed the most attenuated cytotoxicity, but lacked cargo (FITC-Dextran of 10 kDa) delivery ability at the highest working concentration (Figs. S1 and S2*A*). In the following study, we used L9E as the starting template and applied a combined strategy for hydrophobicity balancing between N-terminal and C-terminal domains to discover an endosomal lytic peptide 6 (LP6) with exceptional cargo delivery capacity, and we further demonstrated that conformational sensitivity in anionic environment underlies the mechanism of action of LP6.

Results

An N-terminal hydrophobic domain added to L9E restores its membranolytic activity

Using a previously discovered nontoxic L9E (hereafter termed as lytic peptide 1 - LP1) as the starting template, LP2 (ILILAAKLLKLLKKELKLLK-amide) was designed by adding a random hydrophobic sequence composed of six aliphatic amino acids ILILAA to the N-terminus. To demonstrate the transition of the secondary structures from KL1 to LP1 then to LP2, circular dichroic spectrum analysis was performed. The results showed that while LP1 completely loses helix forming ability from its parent self-aggregating KL1, LP2 obtains an obvious α-helical structure under the same conditions (Fig. 1*A*). This indicates that the appended hydrophobic domain ILILAA allowed the C-terminal domain of L9E to regain helical conformation in an amphipathic environment. To further assess the effect of this structural change on the membranolytic ability of peptide, 20 μM of large unilamellar vesicles (LUVs) that contain calcein were treated with peptides at varying concentrations. The results showed that compared with LP1, the ability of LP2 to lyse liposomal membranes was dramatically enhanced (Fig. 1*B*). However, further experiments showed that LP2 was too toxic to be an ideal delivery vehicle since 2 μM LP2 caused more than 50% cell death after 1 h incubation (Fig. S2*B*). Nevertheless, LP2 with increased membrane activity could serve as the basis for further modulations.

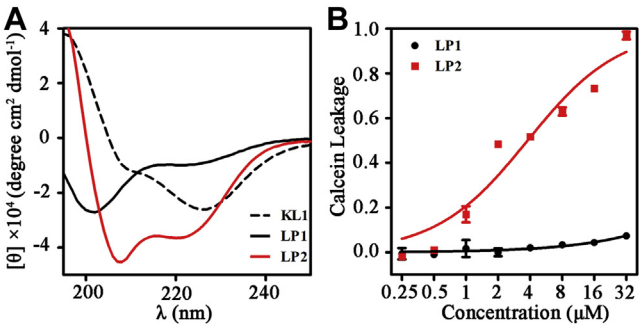

Figure 1. An additional N-terminal hydrophobic domain restores the helix forming ability and membranolytic ability of peptide. *A*, circular dichroism spectra of 75 μM peptide KL1, LP1, and LP2 in PBS buffer in the presence of 10% TFE(v/v). *B*, leakage analysis of peptides against calcein encapsulated vesicles. Serially diluted concentrations of peptides were incubated with calcein encapsulated DOPC/DOPG vesicles (30 μM) in 96-well plates on a gently rocking shaker at room temperature for 1 h. Then, the fluorescence values were measured using a multilabel plate reader. The assays were repeated in triplicates, and data was analyzed with GraphPad Prism 5 as Mean ± SD.

Iterative rebalancing strategy for design and selection of cytosolic delivery peptide

The enhanced ability of LP2 than LP1 to form α-helix in amphipathic environment likely caused LP2's potent lytic activity to cell membrane. To reduce the cytotoxicity of LP2, we went on to tune down the hydrophobicity in the C-terminal helical domain by substituting two Leu to Ala at a time while keeping the N-terminal hydrophobic domain for membrane anchoring. Subsequent adjustments of the N-terminal domain by single amino acid Ile or Leu were taken place to compensate for the loss of hydrophobicity in the helical domain (See Table 1 for all peptide sequences). In this continuous iterative design process, the cytotoxicity and cytosolic delivery ability of the peptides were simultaneously monitored to inform us whether further hydrophobicity adjustment was needed (Figs. S2, *C–F* and 2*A*). When testing the cytosolic delivery ability of the peptides, a concentration close to each peptide's respective IC_{20} value (a safe concentration for delivery purposes) was used. Finally, we obtained a moderately cytotoxic peptide (LP6). Most interestingly, when examined under confocal laser scanning microscope (CLSM), LP6 also showed a significant promotion of cytosolic delivery of FITC-Dextran, with almost 50% of the cells coincubated with LP6 (20 μM) and displayed fluorescence signals homogenously spread in the cytosol and the nucleus (Fig. 2, *A* and *B*-III (compared with I, II)). This cytosolic delivery is obviously different from the influx of FITC-dextran caused by the damage of cell membranes as seen in cells coincubated with 8 μM KL1 (positive control for membrane lysis), in which the nuclei of lysed cells were stained by propidium iodide (PI), and FITC-dextran signals showed vacuole excluded rather than homogenous distribution in the cytosol and concentrated distribution in the nucleoli (Fig. 2*B*-II).

Confirmation of cytosolic delivery ability of LP6

To further confirm the cytosolic delivery ability of LP6 with other biomacromolecules, we used a membrane-impermeable ribosome-inactivation protein, saporin (SAP), as a 28.6 kDa cargo and investigated its delivery efficiency by monitoring the cell death it caused (36). As Figure 3*A* shows, when HeLa cells

Table 1
The sequences of the amphipathic peptides involved in the iterative design

Peptide	Sequences
KL1	KLLKLLKKLLKLLK-amide
LP1 (L9E)	KLLKLLKKELKLLK-amide
LP2	**ILILAA**-KLLKLLKKELKLLK-amide
LP3	**ILILAA**-KLLK*A*LKKE*A*KLLK-amide
LP4	**ILILAA**-KL*A*K*A*LKKE*A*K*A*LK-amide
LP5	**ILILILAA**-KL*A*K*A*LKKE*A*K*A*LK-amide
LP6	**LILILAA**-KL*A*K*A*LKKE*A*K*A*LK-amide

Peptide sequences are shown in one-letter codes for amino acid residues; amide, C-terminal amidation; the italic underlined letters denote the substituting amino acids. The regions set in bold indicate membrane association domains, in contrast to the nonbold amphipathic regions for membrane lysis.

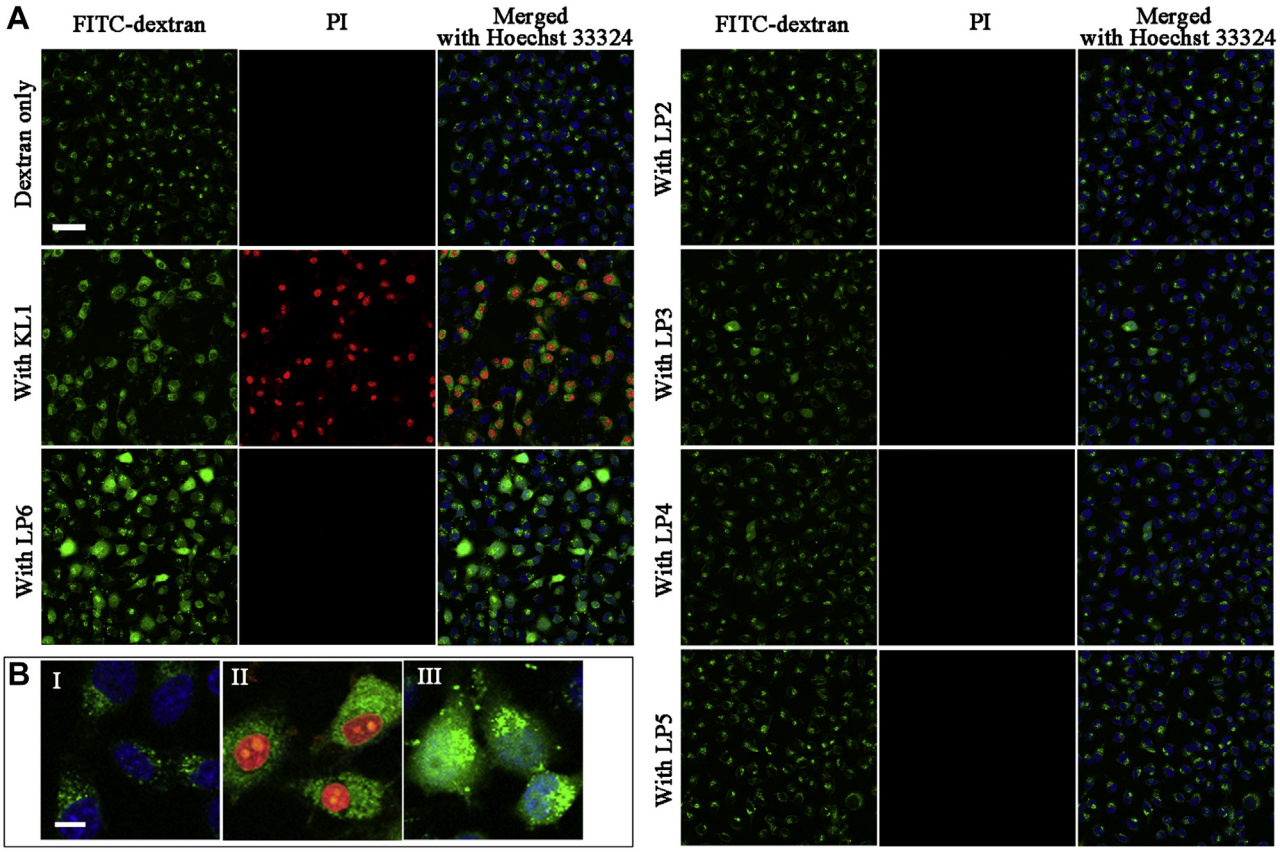

Figure 2. Selection of cytosolic delivery peptide in the iterative design. *A*, images show cytosolic appearance of FITC-dextran (*green*) after treatment with peptides for 1 h. The concentration of the peptide is 8 μM for KL1 or close to the respective IC_{20} value (0.25 μM LP2, 3 μM LP3, 32 μM LP4, 2 μM LP5, 20 μM LP6). All cells were coincubated with propidium iodide (PI, *red*) to indicate cell membrane integrity. Scale bar, 100 μm. *B*, three types of cytosolic appearance of FITC-dextran (*green*) after treatment with peptides and PI (*red*) for 1 h: endosomal entrapment (I); cell membrane leakage (II); cytosolic delivery (III). Scale bar, 100 μm.

were incubated with SAP (10, 20, 50 μg/ml) alone for 60 min, their survival was barely affected. However, in the presence of LP6 (20 μM), apparent cell death was observed with lethality rates of 0.51, 0.63, 0.71, respectively ($p < 0.001$ for all). This indicates a promotive role of LP6 on cytosolic delivery of SAP. Moreover, we evaluated the cytosolic delivery of LP6 on immunoglobulin IgG (150 kDa). HeLa cells were incubated with 200 μg/ml FITC labeled IgG in the presence or absence of LP6 for 60 min. CLSM analysis showed that LP6 can dramatically promote the internalization of IgG (Fig. 3*B*). The cytosolic FITC-IgG signals can be observed in certain cells and indicated that to some extent they were released from the endosomes. Flow cytometry analysis further confirmed that in the presence of LP6, the cellular uptake of FITC-IgG (200 μg/ml) increased by 3.8 folds in 30 min ($p < 0.001$) (Fig. 3*C*). Furthermore, the cytosolic delivery ability of LP6 was also confirmed by CLSM in A549, MCF-7, and HUVEC cells with FITC-dextran as cargo (Fig. 3*D*).

The cytosolic delivery ability of LP6 is related to its moderate hydrophobicity

In order to understand the mechanism behind LP6's delivery ability, we used the grand average of hydropathy (GRAVY) score to quantitate the hydrophobicity of each peptide and arranged the peptides in the order of decreasing hydrophobicity in Table 2. Through this sorting, we found that the cytotoxicity of peptides (characterized by IC_{50} values against HeLa cells) reduces with descending hydrophobicity. We next analyzed the circular dichroism (CD) spectrum of these peptides (Fig. S3*A*). The percentage α-helix of the peptides indicated that the helix forming ability of peptides also decreases as the hydrophobicity decreases (Table 2). The membranolytic ability of peptides assessed by calcein release from liposomes presented the same trend again (Fig. S3*B* and Table 2). Among this set of peptides, LP6 possesses moderate hydrophobicity, along with moderate helix formation ability, membranolytic ability, which leads to a mild cytotoxicity and maximized cytosolic delivery capacity.

LP6-mediated cytosolic delivery involves clathrin-dependent endocytosis

To evaluate the process of LP6-mediated cytosolic delivery of dextran, HeLa cells were incubated with FITC-dextran (250 μg/ml) in the presence of LP6 (20 μM) for 5, 15, 30, and 60 min, respectively. After incubation at each time point, the cell nuclei were stained, and CLSM analysis was performed immediately. The results showed that FITC-dextran is already in a state of diffused distribution in a fraction of cells after

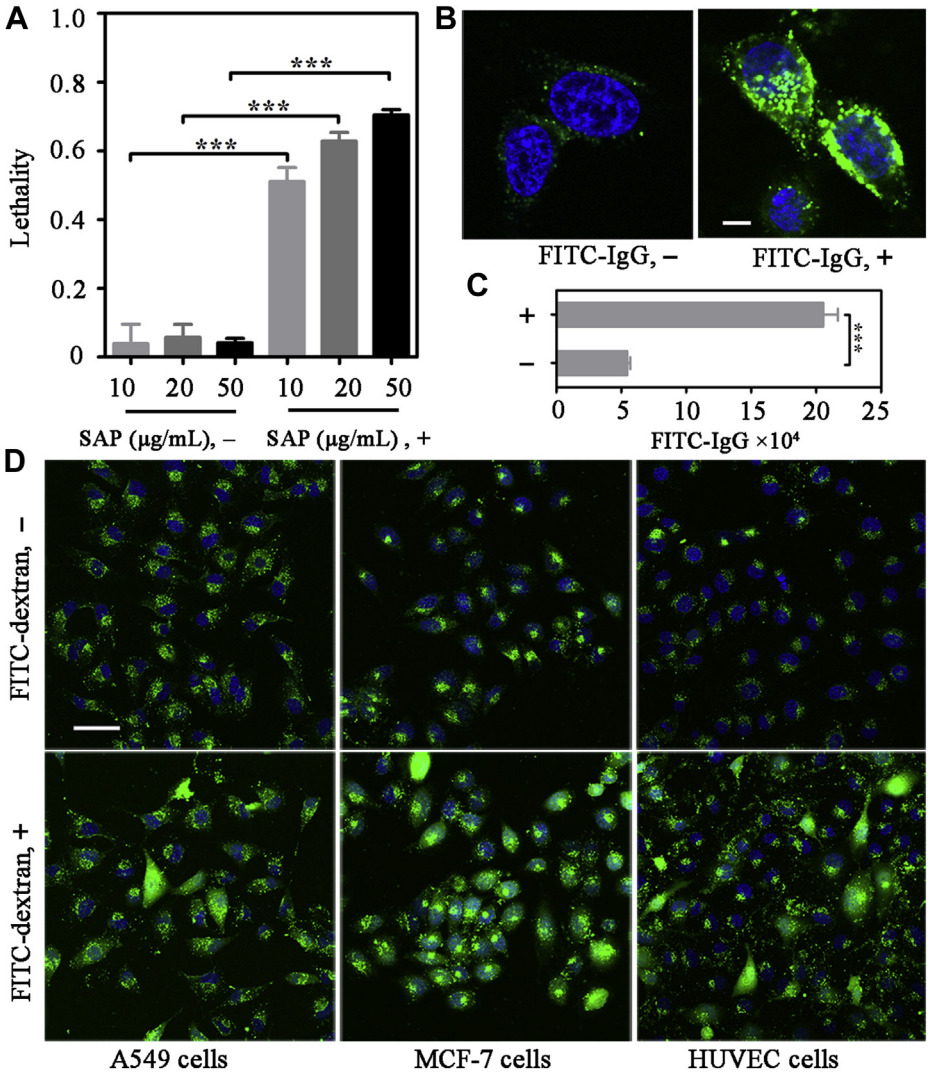

Figure 3. Confirmation of cytosolic delivery ability of LP6. *A*, the promotion effect of LP6 on the cytosolic delivery of saporin. HeLa cells were treated with saporin (10, 20, 50 μg/ml) in the absence (–) or presence (+) of LP6 (20 μM) for 1 h. After incubation, the cells were washed twice with PBS and incubated in DMEM at 37 °C for 6 h. Cytotoxicity was then analyzed by MTT assay. Data presented as mean ± SD of four independent experiments. One-way ANOVA followed by Dunnett's post hoc test. ***$p < 0.001$. *B*, microscopic examination of intracellular appearance of FITC-IgG after treatment without (–) or with (+) LP6 (20 μM) for 1 h. FITC-IgG only was set as a control. *Blue*, Hoechst 33324; *green*, FITC-IgG. Scale bar, 5 μm. *C*, flow cytometry results of cellular uptake of FITC-IgG (200 μg/ml) after treatment without (–)/with (+) LP6 (20 μM) for 30 min. Data presented as mean ± SD of three independent experiments. Student's *t* test. ***$p < 0.001$. *D*, microscopic examination of cytosolic appearance of FITC-dextran in A549, MCF-7, and HUVEC cells after treatment without (–) or with (+) LP6 (20 μM) for 1 h. *Blue*, Hoechst 33324; *green*, FITC-IgG. Scale bar, 50 μm.

Table 2
Hydrophobicity, helix formation ability, membranolytic ability, and cytotoxicity of peptides

Peptide	GRAVY$_{\downarrow}$	α-helix %	LC_{50} (μM)	IC_{50} (μM)
LP2	0.995	~100	3.8	1.3
LP5	0.918	52	7.7	13.0
LP3	0.795	59	7.5	12.5
LP6	0.748	47	11.9	31.1
LP4	0.595	30	>32	>128
LP1	0.529	21	>32	>128

The hydrophobicity of each peptide is characterized by the grand average of hydropathy (GRAVY) score. The helix formation ability is characterized by α-helix % calculated from the mean residue molar ellipticity at 222 nm in PBS buffer in the presence of 10% TFE(v/v). The membranolytic ability is characterized by the half leakage concentration (LC_{50}) value against calcein encapsulated vesicles (30 μM); results are the mean of three independent experiments. The cytotoxicity is characterized by the half inhibitory concentration (IC_{50}) value against HeLa cells; results are the mean of three independent experiments. All peptides are arranged in descending order of hydrophobicity.

5 min of coincubation (Fig. S4). This means that the intracellular release of FITC-dextran is rapid and independent of endosome maturation. To further confirm the involvement of endocytosis in the cytosolic release mediated by LP6, HeLa cells were precultured at 4 °C to suppress energy consumption. Few cytosolic FITC-dextran signals were observed under this treatment, supporting the involvement of endocytosis in this process (Fig. 4*A*). This was further confirmed using flow cytometry analysis. In the presence of LP6, the cellular uptake of FITC-dextran increased by about 2.8 times ($p < 0.001$), yet this effect was significantly weakened ($p < 0.001$) after preincubation at 4 °C for 30 min (Fig. 4*B*).

To further verify the endocytic mechanism, HeLa cells were pretreated with 100 μM amiloride (EIPA, macropinocytosis

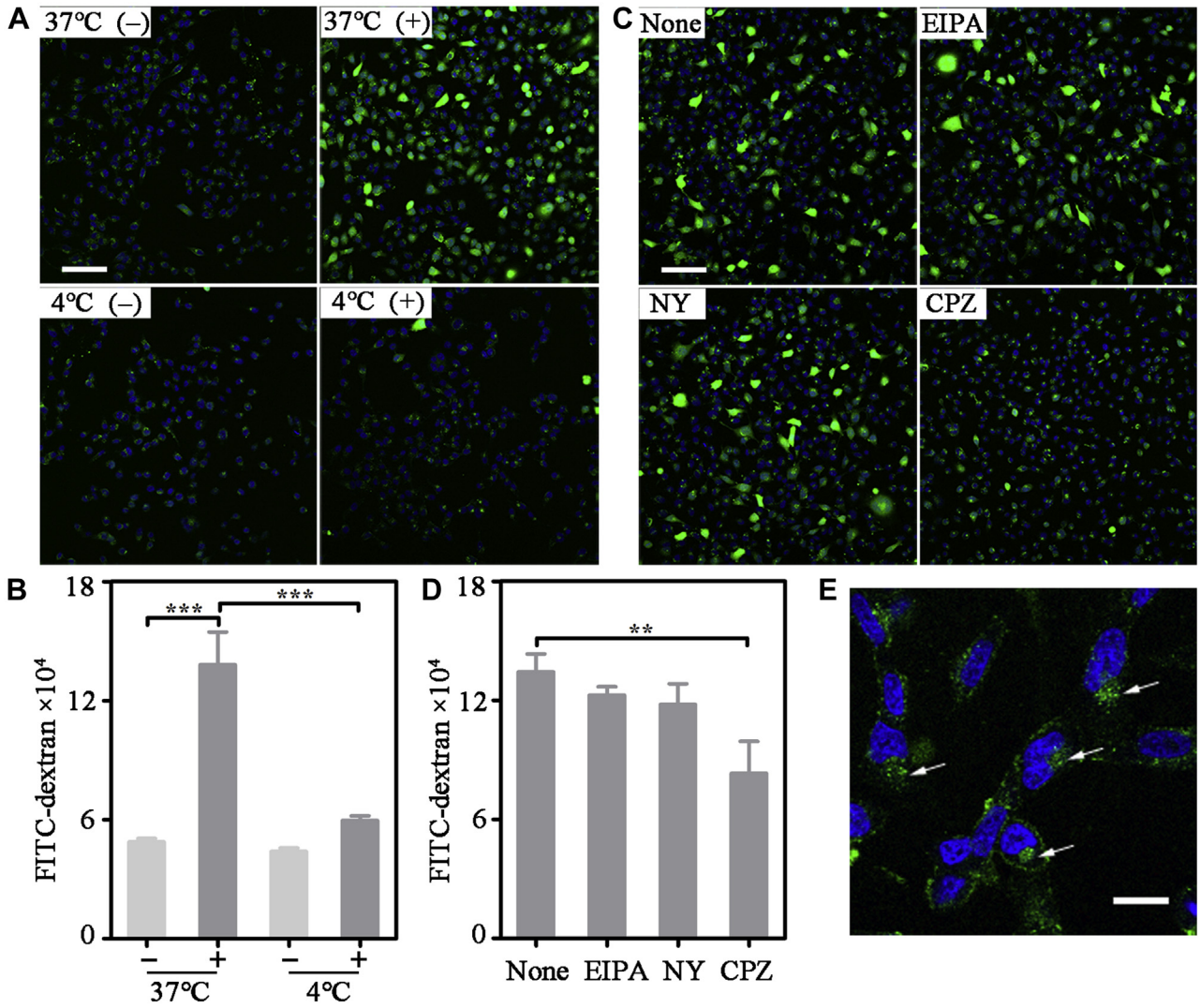

Figure 4. LP6-mediated cytosolic delivery involves clathrin-dependent endocytosis. *A*, cytosolic appearance of FITC-dextran (*green*) after treatment without (–)/with (+) LP6 (20 μM) for 5 min. The cells are precultured at 4 °C or 37 °C for 30 min. Scale bar, 100 μm. *B*, flow cytometry results of cellular uptake of FITC-dextran after treatment without (–)/with (+) LP6 (20 μM) for 5 min. The cells are precultured at 4 °C or 37 °C for 30 min. Data presented as mean ± SD of three independent experiments. One-way ANOVA followed by Dunnett's post hoc test. ***$p < 0.001$. *C*, cytosolic appearance of FITC-dextran (*green*) after treatment with LP6 (20 μM) for 5 min. The cells are pretreated with EIPA, NY, CPZ, or none for 30 min. Scale bar, 100 μm. *D*, flow cytometry results of cellular uptake of FITC-dextran after treatment with LP6 (20 μM) for 5 min. The cells are pretreated with EIPA, NY, CPZ, or none for 30 min. Data presented as mean ± SD of three independent experiments. One-way ANOVA followed by Dunnett's post hoc test. **$p < 0.01$. *E*, intracellular distribution of FITC-L6P. HeLa cells were treated with FITC-L6P (20 μM) for 5 min. The *arrows* indicate the signals around nuclei. Scale bars = 20 μm.

inhibitor), 10 μM nystatin (NY, caveolin-dependent endocytosis inhibitor), or 5 μg/ml chlorpromazine (CPZ, clathrin-mediated endocytosis inhibitor), respectively (26, 37). CLSM analysis showed that the cytosolic delivery of FITC-dextran was significantly inhibited after pretreatment with CPZ, suggesting that clathrin-mediated endocytosis is the primary pathway for FITC-dextran to enter cells with the help of LP6 (Fig. 4*C*). Flow cytometric analysis confirmed this result as the cellular uptake of FITC-dextran was significantly reduced ($p <$ 0.01) after pretreatment with CPZ (Fig. 4*D*).

In addition, LP6 was labeled with FITC for analyzing its behavior under CLSM. As shown in Figure 4*E*, in addition to cell membrane proximal stainings, most FITC-LP6 yielded punctate, dot-like signals around nuclei, indicating that LP6 enters cells through endocytosis under this concentration. And because of its hydrophobicity, LP6 tends to stay on the membranes rather than diffusing into the cytosol. Meanwhile, its endosomal distribution was similar to that of FITC-dextran alone (Fig. 2, *B–I*), suggesting that the cytosolic diffusion of FITC-dextran under coincubation was a result of endosomal lysis caused by LP6.

To evaluate the mechanism by which LP6 promotes the entry of SAP and IgG, MTT assays and imaging experiments were performed respectively. The lethality rates of the groups precultured at 4 °C or pretreated with CPZ (5 μg/ml) dramatically decreased ($p < 0.01$, $p < 0.001$) compared with that of the untreated group, indicating the involvement of clathrin-mediated endocytosis in the cell entry of SAP under the assistance of LP6 (Fig. S5*A*). Precultured at 4 °C or pretreated with CPZ significantly reduced the cellular FITC-IgG

signals, indicating that this involves a clathrin-mediated endocytosis process as well (Fig. S5*B*).

LP6 forms a helical conformation in response to negatively charged phospholipid

Next, we wondered why the moderately hydrophobic LP6 (20 μM) among the series possesses the unique ability to lyse the endosomal membranes without destroying the cell membranes. One of the characteristics of endosomal membranes toward the lumenal side is that they are rich in negatively charged lipids (LBPA or BMP), while the outer leaflet of cell membranes is mostly composed of zwitterionic neutral lipids (38–40). And this difference in the charged states of membranes has recently been used for designing peptides that can promote the endosomal escape of biomacromolecules (23, 26). Therefore, we first evaluated the effect of this difference on the behavior of LP6. DOPC vesicles and DOPC/DOPG vesicles (3:1) were prepared to simulate cell membranes and negatively charged endosomal membranes, respectively, and circular dichroic analysis was performed. As Figure 5*A* shows, LP6 exhibits a disordered conformation in DOPC vesicles, but transforms into an obvious single α-helix structure in DOPC/DOPG vesicles (P/L = 0.25). This suggests that LP6 has higher membrane activity on negatively charged endosomal membranes.

The secondary structures of LP1 to LP5 were analyzed as well (Fig. S6). Figure 5*B* compares the changes in mean residue molar ellipticity of all peptides from with DOPC vesicles to with DOPC/DOPG vesicles at 222 nm, which were arranged in descending order of hydrophobicity from left to right. Interestingly, we found that LP3 and LP6 with medium hydrophobicity showed the strongest anionic lipid sensitivity, while both highly hydrophobic peptides (LP2, LP5) and weakly hydrophobic peptides (LP4, LP1) exhibited significantly reduced anionic lipid sensitivity. Due to the limitation of cytotoxicity, the concentration of LP3 (3 μM) used for cytosolic delivery was much lower than that of LP6 (20 μM). In this context, the conformational response of LP6 to changes in lipid components would be much more significant for membrane perturbation.

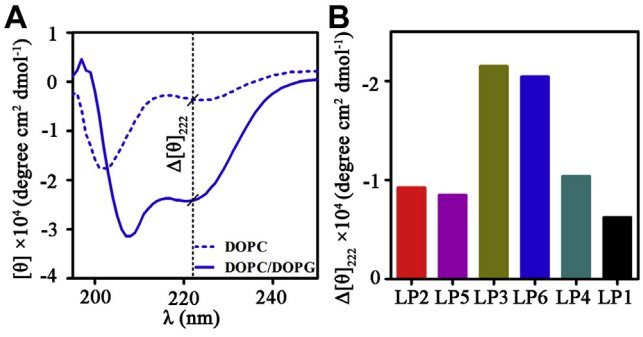

Figure 5. LP6 forms a helical conformation in response to negatively charged phospholipid. *A*, circular dichroism spectra of 75 μM LP6 in PBS buffer that contains 130 mM NaCl in the presence of 200 μM DOPC vesicles or DOPC/DOPG (3:1) vesicles at pH = 7.4. Intersections at 222 nm are highlighted. *B*, the changes in mean residues molar ellipticity of peptides from DOPC vesicles to DOPC-DOPG vesicles at 222 nm. Peptides are arranged in descending order of hydrophobicity.

LP6-mediated cytosolic delivery is related to sialylation modification on endosomal membrane

To resist protease degradation, lysosomal membranes possess the highest degree of glycosylation modification among various biomembranes, and sialic acid originated from these glycosylation modifications can even reach mM levels. Studies revealed that LAMP-1 and LAMP-2, which are estimated to contribute to about 50% of all proteins of the lysosomal membrane, have already appeared in the endosomes (41–44). These facts indicate that the endosomal membranes possess a high degree of glycosylation modification. We postulate that this glycosylation modification results in a higher local concentration of sialic acids in the endosomal membranes relative to the cell membranes and may be another factor that also contributes to peptide's selective damage to endosomal membranes. To investigate the hypothesis, HeLa cells were pretreated with two types of sialyltransferase inhibitor, glycolithocholic acid (Gly-lit) and 3Fax-Peracetyl Neu5Ac (3Fax-Neu5Ac), respectively (45, 46). Sialyltransferases catalyze the transfer of sialic acid residues from the donor substrate CMP-Neu5Ac to acceptor oligosaccharide chains of proteins and lipids (47). CLSM analysis showed that the cytosolic delivery of FITC-dextran by LP6 was significantly inhibited under these treatments, suggesting an important role of sialic acid modifications in this process (Fig. 6*A*). Moreover, an α2-3,6,8,9 Neuraminidase A pretreated group in which the enzyme reduced the sialic acid modifications on cell surface proteins was investigated (48). Results showed that the cytosolic diffusive FITC-dextran signals were unchanged, thus reaffirming that the effector sialic acids were not located on the cell surface but in the endosomes (Fig. 6*A*).

LP6 self-aggregates in response to polysialic acid

While the sialic acid modifications would certainly increase the electrostatic attraction of the cationic peptides to the endosomal membranes, whether this anionic environment could affect the mode of action of peptides by changing their physical state of molecular assembly is unclear. Our previous studies have shown that peptides with a capacity of self-assembly tend to cause direct lysis of the cell membrane (25, 27). To test this assumption, an aggregate incorporation assay was performed. Polysialic acid (PSA) was used to simulate the sialic glycans on the endosomal membrane, and ANS-Na was used as a hydrophobic fluorescent probe (27). The results showed that although LP6 exhibited very weak preassembly in PBS buffer, as the concentration of PSA increased to mM, its self-aggregation dramatically increased (Fig. 6*B*). These suggest that the sialic acid modifications on the endosomal membranes may exert similar effects to the endocytosed LP6.

We also examined the effect of PSA on the assembly behavior of LP1 to LP5 (Fig. S7). The fluorescence values of 128 μM of peptides mixed with ANS-Na under different sialic acid conditions are compared in Figure 6*C*. Not unexpectedly, peptides arranged in the order of hydrophobicity corresponded well with their order of fluorescence intensity—the indicator of their tendency to aggregate in general. Interestingly however, it

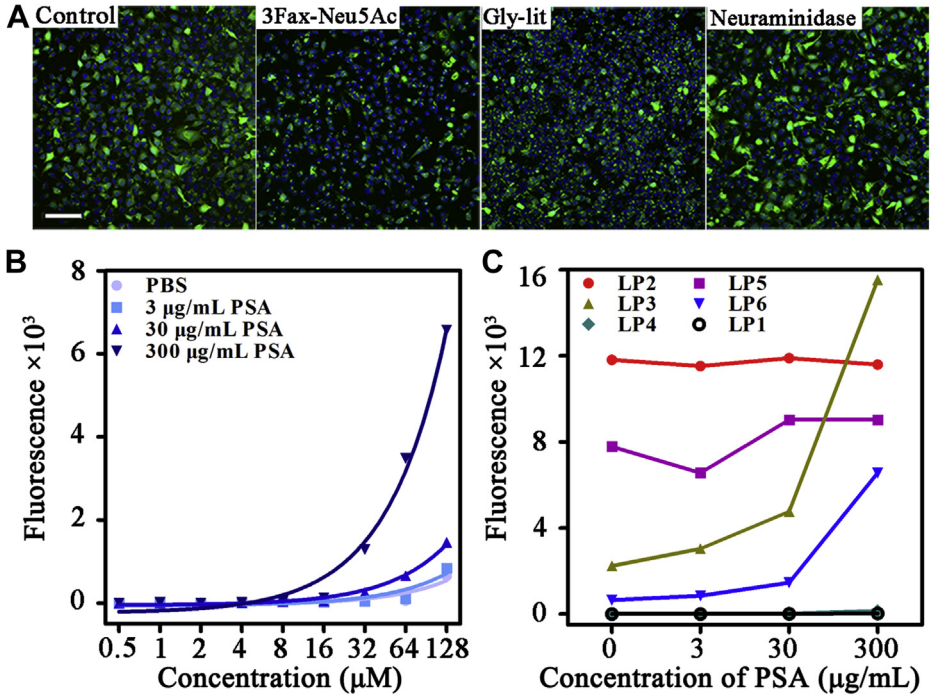

Figure 6. LP6 self-aggregates in response to sialylation modification on endosomal membrane. *A*, LP6-mediated cytosolic delivery is related to sialylation modification on endosomal membrane. Images show cytosolic appearance of FITC-dextran (*green*) after treatment with LP6 (20 μM) for 5 min. The cells were precultured/pretreated with 3Fax-Peracetyl Neu5Ac (3Fax-Neu5Ac) for 3 days, or glycolithocholic acid (Gly-lit) for 5 days or α2-3,6,8,9 Neuraminidase A for 30 min. Scale bar, 100 μm. *B*, self-aggregation of LP6 in PBS buffer in the presence of 0, 3, 30 or 300 μg/ml polysialic acid (PSA) sodium salt. Plots show the 1,8-ANS fluorescence intensity responding to peptide concentration. *C*, self-aggregation of LP1 to LP6 (128 μM) in PBS buffer in the presence of 3, 30, or 300 μg/ml polysialic acid sodium salt. Plots show the 1,8-ANS fluorescence intensity responding to PSA concentration.

was found that these peptides can be divided into three distinct groups based on their response to PSA. The first group comprises LP2 and LP5 with strong hydrophobicity. This type of peptides had already undergone strong, saturated pre-assembly in the PBS buffer. Therefore, their aggregation was barely affected by additional PSA. The second group includes LP1 and LP4, which possess low hydrophobicity. This type of peptides also showed no response to PSA. The last group consists of LP3 and LP6 with moderate hydrophobicity. The assembly state of this group of peptides responded to PSA concentration very sensitively. Again, considering the nontoxic concentration of LP3 allowed for cytosolic delivery is merely 3 μM, the sialic acid responsiveness of LP3 would be insignificant for membrane disruption due to its low concentration.

The pH-sensitive mechanism does not play a significant role in the cytosolic delivery of LP6

The lumen of the endosomes is a relatively acidic environment. However, the effect of pH on LP6's activity was ruled out based on the following results. First, the cytosolic FITC-dextran signals in cells pretreated with bafilomycin A1 (an endosomal acidification inhibitor) were not significantly inhibited (Fig. S8*A*) (24). Second, when the pH of PBS-TFE buffer was adjusted to 5.0, LP6 exhibits reduced rather than enhanced helix forming ability, which was apparently different from the reported pH sensitive endosomolytic peptide GALA (Fig. S8*B*) (49). Other endosomal escaping peptides, such as H5WYG and LAH4-L1, have also been reported to respond to the acidic pH of endosomal lumen, causing the lysis of the endosome membranes (50, 51). Such variances in the mechanisms of action may be caused by the differences in the numbers and relative positions of the pH-sensitive residues. LP6 has a single glutamate residue on the hydrophobic surface, while multiple glutamate or histidine residues of the former peptides appear on the hydrophilic surface. Like LP6, recently reported L17E obtained by single-site substitution of glutamate residue on the hydrophobic surface of M-lycotoxin does not involve pH-sensitive mechanism (26).

Discussion

Collectively, the above results shed light on the mechanism of action of LP6-mediated cytosolic delivery of biomacromolecules as depicted in Figure 7. The hydrophobic domain at the N-terminus allows LP6 to associate with the cell membrane lipids. Meanwhile, the existence of Glu and the replacement of Leu to Ala greatly reduce the helix forming ability of the C-terminal amphiphilic domain. In the extracellular environment, LP6 at a concentration close to IC_{20} is in a monomer state, which will not lead to cell membrane lysis. However, the association of LP6 to membrane triggers endocytic activities *via* clathrin-mediated pathway, allowing the biomacromolecules outside the cell membranes to be taken up into the cells through endosomes together with the peptides. At this stage, the first barrier preventing biomacromolecules from entering the cell has been overcome. Next, in addition to enhanced electrostatic attraction, the negatively charged

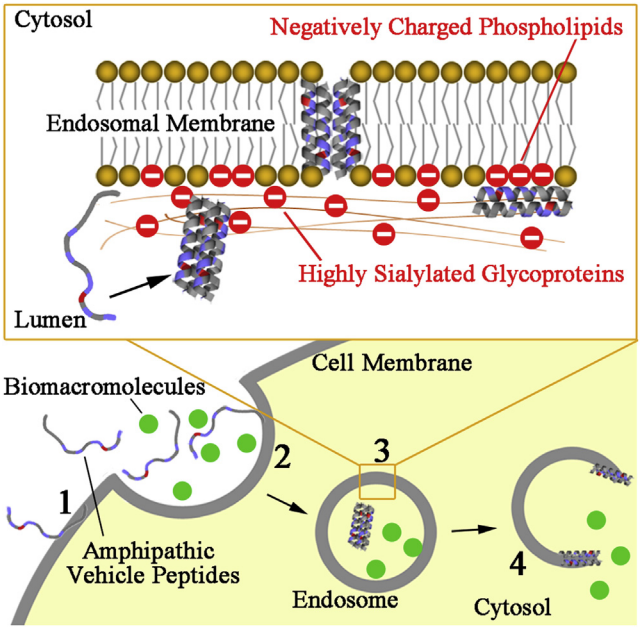

Figure 7. Proposed mechanism of action of LP6. 1, the N-terminal hydrophobic domain increases the affinity of peptide to the cell membrane. 2, LP6 promotes clathrin-mediated endocytosis and cellular uptake of biomacromolecules. 3, LP6 mediates anion-responsive endosomolysis. 4, biomacromolecules are released into the cytosol. Magnified area in (3): In response to the negatively charged phospholipid headgroups and sialic-acid-rich glycoproteins near the membrane of the endosome luminal side, LP6 undergoes helix formation and self-association (*black arrow*), which further leads to local membrane lysis. This environment-sensitive response forms the basis of LP6's unique ability for safe delivery of cargos into cytosol. Color coding for peptide: *gray*, *blue*, and *red* segments represent the relative positions of hydrophobic, hydrophilic, and glutamate residue(s), respectively.

environment brought about by enriched anionic phospholipids and highly sialylated glycoproteins in the endosomal lumen induces the conversion of peptides from random monomers to helices and aggregates that are more capable of disturbing the phospholipid bilayers. Under the synergistic effect of these factors, the endosomal membrane is ruptured, and the biomacromolecules inside can be released into the cytosol.

This study reflects our continued efforts focusing on the precise regulation of hydrophobicity of CAPs for cargo delivery or cancer therapy (27, 52), given that hydrophobicity is regarded as the most important determinant affecting CAPs' membrane activity (18, 19, 53, 54). We hypothesized that the two functionalities dictated by the hydrophobicity of a CAP, *i.e.*, membrane association and membrane lysis, can be separately tuned in one peptide sequence. The initial template peptide LP1 is membrane inactive because the inserted Glu residue disrupted hydrophobic face integrity and created an energy barrier for membrane association. However, adding a 6-aa linear hydrophobic sequence to LP1 led to LP2 with strong cytotoxicity, which indicates the attached hydrophobic sequence, can restore membrane association, hence the lytic activity of the C-terminal amphipathic domain.

This finding prompted us to maintain the framework of LP2 and to further condition the peptide by reducing the hydrophobicity of the lytic domain and compensating the loss of hydrophobicity to the membrane association domain. This iterative process yielded a peptide LP6 with strong delivery capacity and weakened cytotoxicity. Remarkably, LP6 has a medium level of hydrophobicity among the series. Although previous knowledge indicates that strong or weak hydrophobicity is related to the cytotoxicity as well as the self-aggregation of CAPs (27, 55, 56) and that membrane activity of CAPs can change on different phospholipid components (5, 26, 57) or glycosylation (27), how these factors synergize into an integrate mechanism of action of CAPs remained incompletely understood. Here we found that LP6 appeared to have just necessary and sufficient amount of hydrophobicity, which endowed LP6 a unique structure–functional sensitivity to respond to the different anionic environment of cell membrane and endosomal membrane.

This work, together with our previous one (27), constitutes systematic studies on the regulation of peptide membrane activity based on hydrophobicity. The former study discovered that peptides with differently disturbed helical hydrophobic face could cause different modes of cell death, while the work reported here demonstrates that one peptide with optimized hydrophobicity can show selective membrane activities due to the changes in membrane environments. In both works, our practice was the fine-tuning of hydrophobicity, the increment or decrement of which was down to single amino acid resolution. Because of the subtlety in this approach, we believe the observed LP6 conformational behavior and its delivery capability were tightly coupled and indicated a causal relationship.

Although LP6 significantly promotes the internalization of biomacromolecules, there is still room for further optimization of its delivery ability, especially for high-molecule-weight cargos. Dimerization may be a strategy for that purpose, since it has been successfully applied in the design of dfTAT and dfRn (22, 58), although dimerization may also increase cytotoxicity that reduces intracellular delivery (59, 60). Studies have found that for dfRn peptides, a content of 12 arginine residues is an approximate threshold necessary for high endosomal escape efficiency (58). For CAPs, there may also be a threshold for the numbers of cationic residues and hydrophobic residues as well as an optimum ratio between the two. Moreover, the intracellular metabolic stability of LP6 can also be enhanced by replacing L-type amino acids with D isomers, which could lead to prolonged action for endosomolytic delivery.

In summary, the hypothesis proposed and the novel iterative approach applied in this study help discovered a highly efficient vehicle peptide LP6 and further provided mechanistic insights for the precise regulation of CAP's membrane activity. These findings would be instructive for the rational design and modification of more effective vehicle peptides for cytosolic delivery of macromolecular therapeutics, which is much needed given the large number of underexplored intracellular drug targets.

Experimental procedures

Peptide synthesis

All peptides were supplied in pure form by GenScript Ltd. Identities of the peptides were confirmed by reversed-phase

HPLC and electrospray mass spectrometry. And the purity of all peptides tested was more than 95%.

Liposome preparation

Vesicles were made from DOPC or DOPC/DOPG (3:1) (AVT) with an extrusion method. Briefly, lipid was dried from stock solutions in chloroform/methanol (1/1), hydrated with 10 mM PBS buffer, freeze-thawed seven times, and extruded 30 times through an extruder (LE-1, Morgec), equipped with Whatman Nuclepore (GE Healthcare) filters of 100 nm pore size. The final lipid concentration was determined by the Stewart phospholipids assay (61). For calcein leakage experiments, the lipid film was obtained and then hydrated with a 70 mM calcein solution (Adamas-beta), titrated to pH 7.4 with NaOH, and containing 10 mM PBS buffer to make it isotonic to the dilution buffer (PBS 10 mM, pH 7.4, NaCl 130 mM) (62). The liposomes were separated from the unencapsulated dye by performing two gel filtrations on a 10 cm desalting gravity column.

Leakage assay

The leakage assay was carried out according to previous study (62). Vesicles loaded with 70 mM calcein were mixed with peptide solutions of different concentrations in low-adsorption 96-well plates. The final lipid concentration was 30 μM, and the sample volume was 100 μl. The samples were then incubated for 1 h on a gently rocking shaker at room temperature. The fluorescence (F) (485 nm/535 nm) was measured using a multilabel plate reader (Victor X4, PerkinElmer). Vesicles treated without peptide were used as a negative leakage control (F_0) and treated with 0.1% Triton X-100 as a positive leakage control (F_{100}). Leakage was reported as Leakage = $(F - F_0)/(F_{100} - F_0)$. Half leakage concentration (LC_{50}) values were determined using the GraphPad Prism 5 software from semilog curves derived from three independent measurements.

Peptide self-aggregation assay with ANS

Peptide self-aggregation assay with ANS was performed as described in our previous study (27). Briefly, Na-salt of 8-anilino-1-naphthalene sulfonic acid (ANS-Na) (TCI) with a final concentration of 30 μM was mixed with peptide solutions in PBS or PBS with polysialic acid (ChemCruz) in low-adsorption 96-well plates. The total sample volume was 100 μl. After shaking at room temperature for 10 min, the plate was processed in a plate reader (Citation 5, BioTek) to read the fluorescence signal of each well at excitation of 380 nm and emission of 500 nm.

Circular dichroism

CD measurements were performed using a 0.05 cm path length quartz cuvette on a spectropolarimeter (Chirascan-plus, Applied Photophysics) at room temperature. The peptides were dissolved in corresponding buffer: PBS containing 10% TFE (pH 7.4, pH 5.0), 300 μM DOPC vesicles (pH 7.4), 300 μM DOPC/DOPG vesicles (pH 7.4, pH 5.0). Data were collected from 195 to 250 nm (bandwidth, 2 nm; step, 1 nm; repeats, 3). The mean residue molar ellipticities were calculated using the equation $[\theta]_{mr} = \theta_{obs}/(10lcn)$, where θ_{obs} is the measured ellipticity in mdeg, l is the path length in cm, c is the concentration of peptide in M, and n is the number of amino acid residues of the peptide. α-helix % = $-100([\theta]_{222} + 3000)/33{,}000$ (63).

Cell culture

HeLa, A549, MCF-7, HUVEC cells were grown in Dulbecco's modified Eagle's medium (DMEM) (high glucose) supplemented with 10% (v/v) fetal bovine serum (FBS) (Gibco), 100 U/ml penicillin, and 100 μg/ml streptomycin (Beyotime) in a humidified atmosphere containing 5% CO_2.

MTT assay

HeLa cells were transferred into 96-well plates (1×10^4 cells/well) and cultured for 24 h. After complete adhesion, 100 μl of serially diluted concentrations of peptides was added for 1 h at 37 °C. At the end of incubation, peptides were removed, 100 μl fresh media, and 20 μl MTT solution (5 mg/ml in PBS) (Adamas-beta) were added to each well and further incubated at 37 °C for 4 h. Cell viability was determined by dissolving the crystallized MTT with dimethyl sulfoxide (150 μl/well). The absorbance at 490 nm (A) was measured using a multilabel plate reader (Victor X4, PerkinElmer). Cells without the addition of the peptides were set as negative control (A_{con}). Wells with only 100 μl media addition but without cells and peptides were set as blank (A_{bl}). Lethality was calculated using the equation Lethality = $(A_{con} - A)/(A_{con} - A_{bl})$. IC_{50} values were determined using the GraphPad Prism 5 software from semilog curves derived from three independent measurements.

Cellular uptake of 10 kDa dextran and microscopic observation

HeLa cells were transferred into glass-bottomed 24 well plates (4×10^4 cells/well) and cultured for 24 h. After cells adhered to the bottom of the plates, they were washed twice with PBS and then incubated with 250 μg/ml FITC-dextran (10 kDa) (Invitrogen) in the presence of peptides close to IC_{20} concentrations in 400 μl DMEM without FBS for 1 h at 37 °C (26). Cells were washed with PBS, DMEM containing Hoechst 33342 (10 μg/ml) and PI (10 μg/ml) (Beyotime) were added to stain the nucleus for 10 min at 37 °C. Then, they were washed twice with PBS and incubated in fresh DMEM for 3 h at 37 °C. The cellular uptake of FITC-dextran was analyzed in live cells using an FV3000 Olympus confocal laser scanning microscope.

For pulse-chase experiments, the cells were incubated with 250 μg/ml FITC-dextran (10 kDa) (Invitrogen) in the presence of LP6 (20 μM) in 400 μl DMEM without FBS for 5, 15, 30, 60 min at 37 °C. After incubation at each time point, the cells were washed twice with PBS and incubated in DMEM containing Hoechst 33342 (10 μg/ml) to stain the nucleus for 10 min at 37 °C. Observation by CLSM followed immediately.

For the 4 °C experiments, the cells were precultured at 4 °C for 30 min. Then the media were removed, and the cells were washed twice with cold PBS. Fresh cold DMEM containing 20 μM LP6 and 250 μg/ml FITC-dextran were added and the cells were incubated at 4 °C for another 5 min. After incubation, the cells were washed twice with PBS and incubated in DMEM containing Hoechst 33342 (10 μg/ml) to stain the nucleus for 10 min at 37 °C. Observation by CLSM followed.

For the endocytosis inhibitor and acidification inhibitor experiments, the cells were preincubated in DMEM containing 100 μM amiloride (EIPA), 10 μM nystatin (NY), 5 μg/ml chlorpromazine (CPZ), or 200 μM bafilomycin A1 (BafA1) (Solarbio) for 30 min respectively (24, 26, 37). Then, the media were removed and fresh DMEM containing 20 μM LP6 and 250 μg/ml FITC-dextran, as well as corresponding inhibitor, were added and the cells were incubated at 37 °C for 5 min. After incubation, the cells were washed twice with PBS and incubated in DMEM containing Hoechst 33342 (10 μg/ml) to stain the nucleus for 10 min at 37 °C. Observation by CLSM followed.

For the sialyltransferase inhibitor experiments, (1) HeLa cells were transferred into glass-bottomed 24 well plates (2×10^4 cells/well) and cultured for 24 h. After cells adhered to the bottom of the plates, the media were removed and DMEM (with 10% FBS) containing 200 μM glycolithocholic acid (Cayman Chemical) was added for another 3 days (45, 64). Then, the media were removed. Cells were washed twice with PBS. Fresh DMEM containing 20 μM LP6 and 250 μg/ml FITC-dextran were added and the cells were incubated at 37 °C for 5 min. Observation by CLSM followed. (2) HeLa cells were transferred into glass-bottomed 24 well plates (1×10^4 cells/well) and cultured for 24 h. After cells adhered to the bottom of the plates, the media were removed and DMEM (with 10% FBS) containing 400 μM 3Fax-Peracetyl Neu5Ac (Sigma-Aldrich) was added for another 5 days (46). Then, the media were removed. Cells were washed twice with PBS. Fresh DMEM containing 20 μM LP6 and 250 μg/ml FITC-dextran were added and the cells were incubated at 37 °C for 5 min. Observation by CLSM followed.

For the Neuraminidase pretreated experiments, HeLa cells were transferred into glass-bottomed 24 well plates (2×10^4 cells/well) and cultured for 24 h. After cells adhered, they were cultured in DMEM (with 10% FBS) for another 3 days (synchronized with the glycolithocholic acid treated group). Then, the media were removed, 0.1 U/ml α2-3,6,8,9 Neuraminidase A (New England Biolabs) was added and the cells were incubated at 37 °C for 30 min (65). Then, the Neuraminidase was removed. Cells were washed twice with PBS. Fresh DMEM containing 20 μM LP6 and 250 μg/ml FITC-dextran were added and the cells were incubated at 37 °C for 5 min. Observation by CLSM followed.

Intracellular distribution of FITC-LP6

HeLa cells were transferred into glass-bottomed 24 well plates (4×10^4 cells/well) and cultured for 24 h. After cells adhered to the bottom of the plates, they were washed twice with PBS and then incubated with FITC-LP6 (20 μM) for 5 min at 37 °C. Cells were washed with PBS, DMEM containing Hoechst 33342 (10 μg/ml) was added to stain the nucleus for 10 min at 37 °C. Observation by CLSM followed.

Verification of the effect of Neuraminidase pretreatment

In order to confirm that the sialidase pretreatment does reduce the sialic acid modification on the cell surface, we evaluated its effect on the cytotoxicity of KL1, a cationic amphiphilic membranolytic peptide. Briefly, HeLa cells were transferred into 96-well plates (1×10^4 cells/well). After cells were stuck to the bottom of the plates, cells were washed with PBS and pretreated with 0.1 U/ml α2-3,6,8,9 Neuraminidase A at 37 °C for 30 min, while cells without pretreatment were used as the experimental control. Then, 100 μl of serially diluted concentrations of KL1 was added for 1 h at 37 °C. Cells with no peptide addition served as negative controls. MTT assays were performed as mentioned above.

Saporin treatment

HeLa cells were transferred into 96-well plates (1×10^4 cells/well) and cultured for 24 h. After complete adhesion, HeLa cells were treated with 100 μl saporin (Sigma-Aldrich) in the presence or absence of 6 (20 μM) at 37 °C for 1 h. After incubation, the cells were washed twice with PBS and incubated in DMEM at 37 °C for 6 h (26). Cytotoxicity was then analyzed by MTT assay.

For the 4 °C experiments, HeLa cells were precultured at 4 °C for 30 min, then treated with 100 μl saporin (20 μg/ml) in the presence or absence of 6 (20 μM) at 4 °C for 1 h. After incubation, the cells were washed twice with PBS and incubated in DMEM at 37 °C for 6 h. Cytotoxicity was then analyzed by MTT assay.

For the endocytosis inhibitor experiments, the cells were preincubated in DMEM containing 100 μM EIPA, 10 μM NY, or 5 μg/ml CPZ for 30 min respectively. Then, HeLa cells were treated with 100 μl saporin (20 μg/ml) in the presence or absence of 6 (20 μM), as well as corresponding inhibitor, at 37 °C for 1 h. After incubation, the cells were washed twice with PBS and incubated in DMEM at 37 °C for 6 h. Cytotoxicity was then analyzed by MTT assay.

Fluorescent labeling of IgG

Human IgG (Bioss) was diluted with carbonate buffer (25 μM, pH 9.0) to a concentration of 10 mg/ml and then sealed in a dialysis bag. The dialysis bag was put in a 15 ml centrifuge tube, and FITC solution (0.1 mg/ml in carbonate buffer) (Sigma-Aldrich) of ten times the IgG volume was injected. After adding a rotor, the cap of the centrifuge tube was screwed. The centrifuge tube was fixed upside down on a magnetic stirrer under 4 °C. After 24 h of stirring, the IgG solution in the dialysis bag was pipetted, the free FITC was removed by ultrafiltration (4000*g*, 20 min for four times) at 4 °C. Then, the labeled IgG (FITC-IgG) was quantified with a Micro-Volume UV-Vis Spectrophotometer (NanoDrop 2000, Thermo Fisher scientific).

Cellular uptake of IgG and microscopic observation

HeLa cells were transferred into glass-bottomed 24 well plates (4×10^4 cells/well) and cultured for 24 h. After cells adhered to the bottom of the plates, they were washed twice with PBS and then incubated with 100, 200, 500 μg/ml FITC-IgG in the presence of LP6 in DMEM without FBS for 1 h at 37 °C. Cells were washed with PBS and incubated in DMEM for 3 h at 37 °C. The cellular uptake of dextran was analyzed in live cells using an FV3000 Olympus confocal laser scanning microscope.

For the 4 °C experiments, the cells were precultured at 4 °C for 30 min. Then the media were removed, and the cells were washed twice with cold PBS. Fresh cold DMEM containing 20 μM LP6 and 200 μg/ml FITC-IgG were added and the cells were incubated at 4 °C for another 30 min. After incubation, the cells were washed twice with PBS and incubated in DMEM containing Hoechst 33342 (5 μg/ml) to stain the nucleus for 10 min at 37 °C. Observation by CLSM followed.

For the endocytosis inhibitor experiments, the cells were preincubated in DMEM containing 100 μM EIPA, 10 μM NY, or 5 μg/ml CPZ for 30 min respectively. Then, the media were removed and fresh DMEM containing 20 μM LP6 and 200 μg/ml FITC-IgG, as well as corresponding inhibitor, were added and the cells were incubated at 37 °C for 30 min. After incubation, the cells were washed twice with PBS and incubated in DMEM containing Hoechst 33342 (10 μg/ml) to stain the nucleus for 10 min at 37 °C. Observation by CLSM followed.

Flow cytometry analysis

HeLa cells were transferred into 12-well plates (1×10^5 cells/well) and cultured for 24 h. After cells adhered to the bottom of the plates, they were washed twice with PBS.

For cellular uptake of FITC-dextran with the help of LP6, cells were incubated with 250 μg/ml FITC-dextran (10 kDa) (Invitrogen) in the presence of 20 μM LP6 in 1 ml DMEM without FBS for 5 min at 37 °C. After incubation, cells were washed with PBS and incubated with 0.25% trypsin (Beyotime) for 2 min at 37 °C. Then, the cells were transferred to microcentrifuge tubes, centrifuged (1000 rpm, 4 min), and washed once more with PBS. Flow cytometry analysis was performed on 10,000 gated events using Accuri C6 Flow Cytometer (BD). The fluorescence intensity (reported as Mean FL1-A) was recorded.

For the 4 °C experiments, the cells were precultured at 4 °C for 30 min. Then the media were removed, and the cells were washed twice with cold PBS. Fresh cold DMEM containing 20 μM LP6 and 250 μg/ml FITC-dextran were added and the cells were incubated at 4 °C for another 5 min.

For the endocytosis inhibitor experiments, the cells were preincubated in DMEM containing 100 μM EIPA, 10 μM nystatin NY, or 5 μg/ml CPZ for 30 min respectively. Then, the media were removed and fresh DMEM containing 20 μM LP6 and 250 μg/ml FITC-dextran, as well as corresponding inhibitor, were added and the cells were incubated at 37 °C for 5 min.

For cellular uptake of FITC-IgG, cells were incubated with FITC-IgG (200 μg/ml) in the presence of LP6 (20 μM) in 1 ml DMEM without FBS for 30 min at 37 °C. The fluorescence intensity (reported as Mean FL1-A) was recorded.

Statistical analysis

The experimental results are expressed as the means ± standard deviations (or means only) and are accompanied by the number of observations. When group comparisons showed a significant difference, Student's t test or one-way ANOVA test was used. A p value of <0.05 was considered statistically significant.

Data availability

All data are contained within the article and the supporting information.

Supporting information—This article contains supporting information.

Acknowledgments—This work was funded by the National Natural Science Foundation of China (32071393, 81573339, 31170777), the Ministry of Science and Technology of China (2017YFA0205504), the Ministry of Science and Technology of Jiangsu Province (BE2021666), the Bureau of International Cooperation Chinese Academy of Sciences (GJHZ2021136). We are thankful to the Core Facilities of SINANO Nano-Bio-Chem and Biomedicine Division for technical assistances.

Author contributions—X. C. and H. F. formal analysis; X. C., H. L., A. L., and S. J. investigation; H. F. methodology; H. F. resources; X. C. and H. F. writing—original draft.

Conflict of interest—The authors declare that they have no conflicts of interest with the contents of this article.

Abbreviations—The abbreviations used are: 3Fax-Neu5Ac, 3Fax-Peracetyl Neu5Ac; ANS-Na, sodium 8-Anilino-1-naphthalenesulfonate; BafA1, bafilomycin A1; CAPs, cationic amphipathic peptides; CLSM, confocal laser scanning microscope; CMP-Neu5Ac, cytidine 5′-monophospho-N-acetylneuraminic acid; CPP, cell-penetrating peptides; CPZ, chlorpromazine; DOPC, dioleoyl phosphatidylcholine; DOPG, dioleoyl phosphatidylglycerole; EIPA, amiloride; FITC, fluorescein isothiocyanate; Gly-lit, glycolithocholic acid; GRAVY, the grand average of hydropathy; IC_{20}, the 20% inhibitory concentration; IC_{50}, the half inhibitory concentration; IgG, Immunoglobulin G; LAMP-1, lysosomal-associated membrane protein 1; LAMP-2, lysosomal-associated membrane protein 2; LC_{50}, the half leakage concentration; LUVs, large unilamellar vesicles; NY, nystatin; PBS, phosphate buffer saline; PI, propidium iodide; PSA, polysialic acid; SAP, saporin; TFE, 2,2,2-trifluoroethanol.

References

1. Komin, A., Russell, L. M., Hristova, K. A., and Searson, P. C. (2017) Peptide-based strategies for enhanced cell uptake, transcellular transport, and circulation: Mechanisms and challenges. *Adv. Drug Deliv. Rev.* **110**, 52–64

2. Khan, M. M., Filipczak, N., and Torchilin, V. P. (2021) Cell penetrating peptides: A versatile vector for co-delivery of drug and genes in cancer. *J. Control Release* **330**, 1220–1228
3. Sanchez-Navarro, M. (2021) Advances in peptide-mediated cytosolic delivery of proteins. *Adv. Drug Deliv. Rev.* **171**, 187–198
4. Fjell, C. D., Hiss, J. A., Hancock, R. E., and Schneider, G. (2011) Designing antimicrobial peptides: Form follows function. *Nat. Rev. Drug Discov.* **11**, 37–51
5. Sani, M. A., and Separovic, F. (2016) How membrane-active peptides Get into lipid membranes. *Acc. Chem. Res.* **49**, 1130–1138
6. Guha, S., Ghimire, J., Wu, E., and Wimley, W. C. (2019) Mechanistic landscape of membrane-permeabilizing peptides. *Chem. Rev.* **119**, 6040–6085
7. Ramsey, J. D., and Flynn, N. H. (2015) Cell-penetrating peptides transport therapeutics into cells. *Pharmacol. Ther.* **154**, 78–86
8. Futaki, S., and Nakase, I. (2017) Cell-surface interactions on arginine-rich cell-penetrating peptides allow for multiplex modes of internalization. *Acc. Chem. Res.* **50**, 2449–2456
9. Allolio, C., Magarkar, A., Jurkiewicz, P., Baxova, K., Javanainen, M., Mason, P. E., Sachl, R., Cebecauer, M., Hof, M., Horinek, D., Heinz, V., Rachel, R., Ziegler, C. M., Schrofel, A., and Jungwirth, P. (2018) Arginine-rich cell-penetrating peptides induce membrane multilamellarity and subsequently enter via formation of a fusion pore. *Proc. Natl. Acad. Sci. U. S. A.* **115**, 11923–11928
10. Wadia, J. S., Stan, R. V., and Dowdy, S. F. (2004) Transducible TAT-HA fusogenic peptide enhances escape of TAT-fusion proteins after lipid raft macropinocytosis. *Nat. Med.* **10**, 310–315
11. Dixon, J. E., Osman, G., Morris, G. E., Markides, H., Rotherham, M., Bayoussef, Z., El Haj, A. J., Denning, C., and Shakesheff, K. M. (2016) Highly efficient delivery of functional cargoes by the synergistic effect of GAG binding motifs and cell-penetrating peptides. *Proc. Natl. Acad. Sci. U. S. A.* **113**, E291–E299
12. Zasloff, M. (2002) Antimicrobial peptides of multicellular organisms. *Nature* **415**, 389–395
13. Hancock, R. E., and Sahl, H. G. (2006) Antimicrobial and host-defense peptides as new anti-infective therapeutic strategies. *Nat. Biotechnol.* **24**, 1551–1557
14. Nguyen, L. T., Haney, E. F., and Vogel, H. J. (2011) The expanding scope of antimicrobial peptide structures and their modes of action. *Trends Biotechnol.* **29**, 464–472
15. Ageitos, J. M., Sanchez-Perez, A., Calo-Mata, P., and Villa, T. G. (2017) Antimicrobial peptides (AMPs): Ancient compounds that represent novel weapons in the fight against bacteria. *Biochem. Pharmacol.* **133**, 117–138
16. Mookherjee, N., Anderson, M. A., Haagsman, H. P., and Davidson, D. J. (2020) Antimicrobial host defence peptides: Functions and clinical potential. *Nat. Rev. Drug Discov.* **19**, 311–332
17. Shai, Y. (2002) Mode of action of membrane active antimicrobial peptides. *Biopolymers* **66**, 236–248
18. Brogden, K. A. (2005) Antimicrobial peptides: Pore formers or metabolic inhibitors in bacteria? *Nat. Rev. Microbiol.* **3**, 238–250
19. Hale, J. D., and Hancock, R. E. (2007) Alternative mechanisms of action of cationic antimicrobial peptides on bacteria. *Expert Rev. Anti Infect. Ther.* **5**, 951–959
20. Hoskin, D. W., and Ramamoorthy, A. (2008) Studies on anticancer activities of antimicrobial peptides. *Biochim. Biophys. Acta* **1778**, 357–375
21. Baxter, A. A., Lay, F. T., Poon, I. K. H., Kvansakul, M., and Hulett, M. D. (2017) Tumor cell membrane-targeting cationic antimicrobial peptides: Novel insights into mechanisms of action and therapeutic prospects. *Cell. Mol. Life Sci.* **74**, 3809–3825
22. Erazo-Oliveras, A., Najjar, K., Dayani, L., Wang, T. Y., Johnson, G. A., and Pellois, J. P. (2014) Protein delivery into live cells by incubation with an endosomolytic agent. *Nat. Methods* **11**, 861–867
23. Azuma, Y., Imai, H., Kawaguchi, Y., Nakase, I., Kimura, H., and Futaki, S. (2018) Modular redesign of a cationic lytic peptide to promote the endosomal escape of biomacromolecules. *Angew. Chem. Int. Ed. Engl.* **57**, 12771–12774
24. Arafiles, J. V. V., Hirose, H., Akishiba, M., Tsuji, S., Imanishi, M., and Futaki, S. (2020) Stimulating macropinocytosis for intracellular nucleic acid and protein delivery: A combined strategy with membrane-lytic peptides to facilitate endosomal escape. *Bioconjug. Chem.* **31**, 547–553
25. Liu, X., Cao, R., Wang, S., Jia, J., and Fei, H. (2016) Amphipathicity determines different cytotoxic mechanisms of lysine- or arginine-rich cationic hydrophobic peptides in cancer cells. *J. Med. Chem.* **59**, 5238–5247
26. Akishiba, M., Takeuchi, T., Kawaguchi, Y., Sakamoto, K., Yu, H. H., Nakase, I., Takatani-Nakase, T., Madani, F., Graslund, A., and Futaki, S. (2017) Cytosolic antibody delivery by lipid-sensitive endosomolytic peptide. *Nat. Chem.* **9**, 751–761
27. Chen, X., Ji, S., Li, A., Liu, H., and Fei, H. (2020) Toggling preassembly with single-site mutation switches the cytotoxic mechanism of cationic amphipathic peptides. *J. Med. Chem.* **63**, 1132–1141
28. Castelletto, V., Barnes, R. H., Karatzas, K. A., Edwards-Gayle, C. J. C., Greco, F., Hamley, I. W., Rambo, R., Seitsonen, J., and Ruokolainen, J. (2018) Arginine-containing surfactant-like peptides: Interaction with lipid membranes and antimicrobial activity. *Biomacromolecules* **19**, 2782–2794
29. Chen, C., Li, G., Cui, X., Chen, J., Yu, Q., Zong, C., Zhao, Y., Xu, M., Zhou, S., and Xu, H. (2020) Mechanistic investigation of a self-assembling peptide against Escherichia coli. *Langmuir* **36**, 9800–9809
30. Javadpour, M. M., Juban, M. M., Lo, W. C., Bishop, S. M., Alberty, J. B., Cowell, S. M., Becker, C. L., and McLaughlin, M. L. (1996) De novo antimicrobial peptides with low mammalian cell toxicity. *J. Med. Chem.* **39**, 3107–3113
31. Sinthuvanich, C., Veiga, A. S., Gupta, K., Gaspar, D., Blumenthal, R., and Schneider, J. P. (2012) Anticancer beta-hairpin peptides: Membrane-induced folding triggers activity. *J. Am. Chem. Soc.* **134**, 6210–6217
32. Khara, J. S., Obuobi, S., Wang, Y., Hamilton, M. S., Robertson, B. D., Newton, S. M., Yang, Y. Y., Langford, P. R., and Ee, P. L. R. (2017) Disruption of drug-resistant biofilms using de novo designed short alpha-helical antimicrobial peptides with idealized facial amphiphilicity. *Acta Biomater.* **57**, 103–114
33. Turner, J., Cho, Y., Dinh, N. N., Waring, A. J., and Lehrer, R. I. (1998) Activities of LL-37, a cathelin-associated antimicrobial peptide of human neutrophils. *Antimicrob. Agents Chemother.* **42**, 2206–2214
34. Habermann, E. (1972) Bee and wasp venoms. *Science* **177**, 314–322
35. Yan, L., and Adams, M. E. (1998) Lycotoxins, antimicrobial peptides from venom of the wolf spider Lycosa carolinensis. *J. Biol. Chem.* **273**, 2059–2066
36. Bolognesi, A., Tazzari, P. L., Olivieri, F., Polito, L., Falini, B., and Stirpe, F. (1996) Induction of apoptosis by ribosome-inactivating proteins and related immunotoxins. *Int. J. Cancer* **68**, 349–355
37. Qiu, Y., Chow, M. Y. T., Liang, W., Chung, W. W. Y., Mak, J. C. W., and Lam, J. K. W. (2017) From pulmonary surfactant, synthetic KL4 peptide as effective siRNA delivery vector for pulmonary delivery. *Mol. Pharm.* **14**, 4606–4617
38. Matsuo, H., Chevallier, J., Mayran, N., Le Blanc, I., Ferguson, C., Faure, J., Blanc, N. S., Matile, S., Dubochet, J., Sadoul, R., Parton, R. G., Vilbois, F., and Gruenberg, J. (2004) Role of LBPA and Alix in multivesicular liposome formation and endosome organization. *Science* **303**, 531–534
39. van Meer, G., Voelker, D. R., and Feigenson, G. W. (2008) Membrane lipids: Where they are and how they behave. *Nat. Rev. Mol. Cell Biol.* **9**, 112–124
40. Kobayashi, T., Stang, E., Fang, K. S., de Moerloose, P., Parton, R. G., and Gruenberg, J. (1998) A lipid associated with the antiphospholipid syndrome regulates endosome structure and function. *Nature* **392**, 193–197
41. Akasaki, K., Michihara, A., Fujiwara, Y., Mibuka, K., and Tsuji, H. (1996) Biosynthetic transport of a major lysosome-associated membrane glycoprotein 2, LAMP-2: A significant fraction of newly synthesized LAMP-2 is delivered to lysosomes by way of early endosomes. *J. Biochem.* **120**, 1088–1094
42. Cook, N. R., Row, P. E., and Davidson, H. W. (2004) Lysosome associated membrane protein 1 (Lamp1) traffics directly from the TGN to early endosomes. *Traffic* **5**, 685–699
43. Eskelinen, E. L. (2006) Roles of LAMP-1 and LAMP-2 in lysosome biogenesis and autophagy. *Mol. Aspects Med.* **27**, 495–502
44. Wreden, C. C., Wlizla, M., and Reimer, R. J. (2005) Varied mechanisms underlie the free sialic acid storage disorders. *J. Biol. Chem.* **280**, 1408–1416

45. Chang, K. H., Lee, L., Chen, J., and Li, W. S. (2006) Lithocholic acid analogues, new and potent alpha-2,3-sialyltransferase inhibitors. *Chem. Commun. (Camb.)*. https://doi.org/10.1039/b514915k
46. Rillahan, C. D., Antonopoulos, A., Lefort, C. T., Sonon, R., Azadi, P., Ley, K., Dell, A., Haslam, S. M., and Paulson, J. C. (2012) Global metabolic inhibitors of sialyl- and fucosyltransferases remodel the glycome. *Nat. Chem. Biol.* **8**, 661–668
47. Wang, L., Liu, Y., Wu, L., and Sun, X. L. (2016) Sialyltransferase inhibition and recent advances. *Biochim. Biophys. Acta* **1864**, 143–153
48. Ishikawa, K., Medina, S. H., Schneider, J. P., and Klar, A. J. S. (2017) Glycan alteration imparts cellular resistance to a membrane-lytic anticancer peptide. *Cell Chem. Biol.* **24**, 149–158
49. Subbarao, N. K., Parente, R. A., Szoka, F. C., Jr., Nadasdi, L., and Pongracz, K. (1987) pH-dependent bilayer destabilization by an amphipathic peptide. *Biochemistry* **26**, 2964–2972
50. Midoux, P., Kichler, A., Boutin, V., Maurizot, J. C., and Monsigny, M. (1998) Membrane permeabilization and efficient gene transfer by a peptide containing several histidines. *Bioconjug. Chem.* **9**, 260–267
51. Wolf, J., Aisenbrey, C., Harmouche, N., Raya, J., Bertani, P., Voievoda, N., Suss, R., and Bechinger, B. (2017) pH-dependent membrane interactions of the histidine-rich cell-penetrating peptide LAH4-L1. *Biophys. J.* **113**, 1290–1300
52. Ji, S. S., Yang, X. Z., Chen, X. L., Li, A., Yan, D. D., Xu, H. Y., and Fei, H. (2020) Structure-tuned membrane active Ir-complexed oligoarginine overcomes cancer cell drug resistance and triggers immune responses in mice. *Chem. Sci.* **11**, 9126–9133
53. Shai, Y. (1999) Mechanism of the binding, insertion and destabilization of phospholipid bilayer membranes by alpha-helical antimicrobial and cell non-selective membrane-lytic peptides. *Biochim. Biophys. Acta* **1462**, 55–70
54. Wimley, W. C. (2010) Describing the mechanism of antimicrobial peptide action with the interfacial activity model. *ACS Chem. Biol.* **5**, 905–917
55. Chen, Y., Guarnieri, M. T., Vasil, A. I., Vasil, M. L., Mant, C. T., and Hodges, R. S. (2007) Role of peptide hydrophobicity in the mechanism of action of alpha-helical antimicrobial peptides. *Antimicrob. Agents Chemother.* **51**, 1398–1406
56. Wang, J., Liu, K., Xing, R., and Yan, X. (2016) Peptide self-assembly: Thermodynamics and kinetics. *Chem. Soc. Rev.* **45**, 5589–5604
57. Epand, R. M., and Epand, R. F. (2011) Bacterial membrane lipids in the action of antimicrobial agents. *J. Pept. Sci.* **17**, 298–305
58. Najjar, K., Erazo-Oliveras, A., Mosior, J. W., Whitlock, M. J., Rostane, I., Cinclair, J. M., and Pellois, J. P. (2017) Unlocking endosomal entrapment with supercharged arginine-rich peptides. *Bioconjug. Chem.* **28**, 2932–2941
59. Nomura, Y., Sakamoto, K., Akishiba, M., Iwata, T., Hirose, H., and Futaki, S. (2020) Improved cytosolic delivery of macromolecules through dimerization of attenuated lytic peptides. *Bioorg. Med. Chem. Lett.* **30**, 127362
60. Hyun, S., Lee, S., Kim, S., Jang, S., Yu, J., and Lee, Y. (2014) Apoptosis inducing, conformationally constrained, dimeric peptide analogs of KLA with submicromolar cell penetrating abilities. *Biomacromolecules* **15**, 3746–3752
61. Stewart, J. C. (1980) Colorimetric determination of phospholipids with ammonium ferrothiocyanate. *Anal. Biochem.* **104**, 10–14
62. Hovakeemian, S. G., Liu, R., Gellman, S. H., and Heerklotz, H. (2015) Correlating antimicrobial activity and model membrane leakage induced by nylon-3 polymers and detergents. *Soft Matter* **11**, 6840–6851
63. Nielsen, S. L., Frimodt-Moller, N., Kragelund, B. B., and Hansen, P. R. (2007) Structure–activity study of the antibacterial peptide fallaxin. *Protein Sci.* **16**, 1969–1976
64. Moon, S. C., Joo, S. Y., Chung, T. W., Choi, H. J., Park, M. J., Bae, S. J., Kim, K. J., Kim, C. H., Joo, M., and Ha, K. T. (2016) Abiotic stress of ambient cold temperature regulates the host receptivity to pathogens by cell surfaced sialic acids. *Biochem. Biophys. Res. Commun.* **476**, 159–166
65. Han, Y. Y., Liu, H. Y., Han, D. J., Zong, X. C., Zhang, S. Q., and Chen, Y. Q. (2013) Role of glycosylation in the anticancer activity of antibacterial peptides against breast cancer cells. *Biochem. Pharmacol.* **86**, 1254–1262